Robust topology optimization of structures with imperfect geometry based on geometric nonlinear analysis

M. Jansen[a], G. Lombaert[a], M. Schevenels[b]

[a]*Department of Civil Engineering, KU Leuven, Kasteelpark Arenberg 40, B-3001 Leuven, Belgium*
[b]*Department of Architecture, KU Leuven, Kasteelpark Arenberg 1, B-3001 Leuven, Belgium*

Abstract

Topology optimization often leads to structures consisting of slender elements which are particularly sensitive to geometric imperfections. Such imperfections might affect the structural stability and induce large displacement effects in these slender structures. This paper therefore presents a robust approach to topology optimization which accounts for geometric imperfections and their potentially detrimental influence on the structural stability. Geometric nonlinear effects are incorporated in the optimization by means of a Total Lagrangian finite element formulation in the minimization of end-compliance. Geometric imperfections are modeled as a vector-valued random field in the design domain. The resulting uncertain performance of the design is taken into account by minimizing a weighted sum of the mean and standard deviation of the compliance in the robust optimization problem. These stochastic moments are typically estimated by means of sampling methods such as Monte Carlo simulation. However, these methods require multiple independent nonlinear finite element analyses in each design iteration of the optimization algorithm. An efficient solution algorithm which uses adjoint differentiation in a second-order perturbation method is therefore developed to estimate the stochastic moments during the optimization. Two applications with structures that exhibit different types of structural instabilities are examined. In both cases, it is demonstrated by means of an extensive

Email address: geert.lombaert@bwk.kuleuven.be (G. Lombaert)

Postprint submitted to Computer Methods in Applied Mechanics and Engineering
Published version: M. Jansen, M. Schevenels, and G. Lombaert. Robust topology optimization of structures with imperfect geometry based on geometric nonlinear analysis. *Computer Methods in Applied Mechanics and Engineering*, 285:452-467, 2015. http://dx.doi.org/10.1016/j.cma.2014.11.028

Monte Carlo simulation that the deterministic design is very sensitive to imperfections, while the design obtained my means of the proposed method is much more robust.

Keywords: Topology Optimization, Geometric Nonlinearity, Robust Optimization, Stochastic Perturbation Method

---

1. Introduction

Topology optimization is a structural optimization technique which seeks the best layout for a structure by optimizing the material distribution in a predefined design domain. The popularity of the method is demonstrated by its widespread application in various fields of engineering as outlined in a number of recent review papers [1, 2]. Topology optimization often provides an innovative and highly efficient solution for the design problem at hand.

However, the robustness of the optimized design remains an important concern since there is always a level of uncertainty involved with respect to the problem specifications, and minor variations in the physical system might result in a strongly deteriorated performance or even render the design infeasible. Robust optimization takes into account these uncertainties in the optimization in order to find designs which are both efficient and robust. Different sources of uncertainty that are relevant in structural design have been considered in robust topology optimization including variable loads (e.g. [3, 4, 5]), uncertain material properties (e.g. [6, 7]), and geometric imperfections (e.g. [8, 9, 10, 11, 12]).

This paper focuses on robust topology optimization accounting for geometric imperfections. Topology optimization in mechanical applications often results in slender structures which are sensitive to geometric imperfections. Structural members under compression are particularly sensitive as the influence of initial imperfections is magnified by nonlinear effects and even the structure's global stability might be affected. Despite their relevance in practical design problems, these issues have not yet received much attention in continuum topology optimization. Jalalpour et al. [13] presented a robust approach to truss topology design which takes into account the influence of imperfections on the structural stability by means of an approximate scheme for the redistribution of forces. Lazarov et al. [14] incorporated a nonlinear finite element formulation in the robust design of a large displacement mechanism affected by etching imperfections. A stochastic collocation

method with a limited number of collocation points was used to mitigate the computational cost of the method.

In accordance with the literature on topology optimization of geometric nonlinear structures [15, 16], this work incorporates geometric nonlinear phenomena in the optimization by means of a Total Lagrangian formulation for large displacement mechanics. A probabilistic approach to robust optimization is adopted: probability distributions are assigned to the uncertainties and the robust performance of a design is assessed in terms of stochastic moments such as the mean and standard deviation. A stochastic perturbation method is developed as an alternative to sampling or quadrature methods such as Monte Carlo simulation in order to estimate these stochastic moments without having to solve multiple instances of the nonlinear equilibrium equations in each design iteration of the robust optimization.

The paper is organized as follows. The first part briefly reviews density-based topology optimization for mechanical structures including standard techniques such as the SIMP method and projection filters. The extension of the problem formulation to structures exhibiting geometric nonlinearity is also considered. The second part then proceeds with the probabilistic approach to robust topology optimization accounting for imperfections: a random field model for geometric imperfections in the design domain is established, the formulation of the robust optimization problem is discussed, and a solution strategy based on the stochastic perturbation method is developed. Finally, two applications of the robust approach are presented: the design of a shallow arch and a pinned column-like structure. Both structures consist of slender members acting under compression; however, these structures exhibit different types of critical points (i.e. bifurcation and limit point instabilities) which have an important impact on the imperfection sensitivity [17].

2. Topology optimization of geometric nonlinear structures

2.1. Density-based topology optimization

Topology optimization determines the best structural layout by optimizing the material distribution in a design domain Ω for a given set of constraints and boundary conditions. This work follows a density-based approach to topology optimization. The design domain Ω is discretized by means of n_e finite elements and the structure is parameterized by assigning a physical material density $\bar{\rho}_e$ to each element in the design domain [18].

The volume densities indicate whether material is present ($\bar{\rho}_e = 1$) or absent ($\bar{\rho}_e = 0$). The volume fraction of the design domain occupied by the structure is therefore expressed as:

$$V = \frac{1}{V_\Omega} \sum_{e=1}^{n_\mathrm{e}} v_e \bar{\rho}_e \tag{1}$$

where v_e is the volume of element e and $V_\Omega = \sum_{e=1}^{n_\mathrm{e}} v_e$ is the volume of the design domain. Formulating topology optimization in terms of decision variables $\bar{\rho}_e$ that can only take on $0/1$ values leads to an integer programming problem which is very hard to solve. The problem is therefore formulated as a nonlinear programming problem by allowing the volume densities to vary continuously between the material and void phase (i.e. $0 \leq \bar{\rho}_e \leq 1$). In this way, the optimization problem can be solved efficiently by means of a gradient-based optimization algorithm. However, intermediate densities ($0 < \bar{\rho}_e < 1$) usually lack a physical interpretation and should be avoided in the optimized design. The well-known Solid Isotropic Material with Penalization (SIMP) method [19, 20] is used in this paper in order to penalize intermediate densities in the interpolation between material density and stiffness:

$$E_e = E_{\min} + (E_0 - E_{\min})\, \bar{\rho}_e^p \tag{2}$$

where E_0 and $E_{\min}$ are the Young's moduli of the material and void phase, respectively. A very small non-zero stiffness $E_{\min}$ is assigned to the void phase in order to prevent singularities in the elasticity problem. Intermediate densities are made inefficient by selecting the penalization parameter $p > 1$.

In this paper, the formulation of the optimization problem further relies on projection filters [21, 22, 23] for solving issues such as mesh-dependence of the optimal solution. Projection filters can be used to impose a minimum length scale in the design and even serve as a simplified model for incorporating certain manufacturing processes [24]. When projection filters are applied, new design variables ρ_e are assigned to every element and the physical densities $\bar{\rho}_e$ are defined as a function of these design variables ρ_e in two steps. The design variables ρ_e are first smoothed by a density filter [25, 26] to obtain the intermediate densities $\tilde{\rho}_e$:

$$\tilde{\rho}_e = \frac{\sum_{i=1}^{n_\mathrm{e}} \kappa_{ei} v_i \rho_i}{\sum_{i=1}^{n_\mathrm{e}} \kappa_{ei} v_i}, \qquad \kappa_{ei} = \max(R - \|\mathbf{x}_e - \mathbf{x}_i\|_2, 0) \tag{3}$$

where $\mathbf{x}_e$ are the coordinates of the center of element e and the filter radius R is related to the desired minimum length scale in the structure.

The smoothing operation (3) removes rapid variations in the design variables, but also introduces unwanted gray transition zones between material and void phase. Gray elements are removed in the second step by projecting the intermediate variables $\tilde{\rho}_e$ using a regularized Heaviside function [10, 21]:

$$\bar{\rho}_e = \frac{\tanh(\beta\eta) + \tanh(\beta(\tilde{\rho}_e - \eta))}{\tanh(\beta\eta) + \tanh(\beta(1-\eta))} \tag{4}$$

where the parameter β determines the steepness of the function and $\eta \in [0;1]$ is the threshold value of the projection.

Minimum compliance is commonly considered as the basic design problem for mechanical structures. The goal is to find the design which minimizes the work done by the external forces for a limited amount of material:

$$\begin{aligned} \min_{\boldsymbol{\rho}} \quad & f(\boldsymbol{\rho}) = \mathbf{P}^{\mathsf{T}}\mathbf{u}(\boldsymbol{\rho}) \\ \text{s.t.} \quad & V(\boldsymbol{\rho}) - V_{\max} \leq 0 \\ & \mathbf{0} \leq \boldsymbol{\rho} \leq \mathbf{1} \end{aligned} \tag{5}$$

where the vector $\boldsymbol{\rho} \in \mathbb{R}^{n_e}$ collects all the individual design variables ρ_e. The volume fraction $V(\boldsymbol{\rho})$ of the design is limited to a certain value $V_{\max}$. The nodal load vector $\mathbf{P}$ contains the discretized external forces. The nodal displacements $\mathbf{u}$ of design $\boldsymbol{\rho}$ are determined by means of a finite element analysis. When small strains and displacements are assumed, this amounts to solving the following linear system:

$$\mathbf{g}_{\mathrm{l}}(\boldsymbol{\rho}, \mathbf{u}) = \mathbf{K}(\boldsymbol{\rho})\mathbf{u} - \mathbf{P} = \mathbf{0} \tag{6}$$

The linear stiffness matrix $\mathbf{K}(\boldsymbol{\rho})$ is assembled from the element stiffness matrices $\mathbf{K}_e(\boldsymbol{\rho}) = E_e(\boldsymbol{\rho})\mathbf{K}_e^0$ where $\mathbf{K}_e^0$ is the element stiffness matrix for unit-stiffness.

Finally, the optimization problems in this paper are solved by means of the method of moving asymptotes [27] while the design sensitivities required by the algorithm are computed by means of adjoint differentiation [28].

2.2. Geometric nonlinearity

In this paper the natural extension of the minimum compliance problem is considered in order to incorporate buckling and other geometric nonlinear effects in the optimization. The optimization problem is still formulated as in Eq. (5); however, the equilibrium equations are replaced by a

Total Lagrangian finite element formulation for large displacements analysis. This modified optimization problem is often referred to as minimum end-compliance [15, 29] since the objective function $f = \mathbf{P}^{\mathsf{T}}\mathbf{u}$ no longer corresponds to the external work. In the following, linear compliance and nonlinear end-compliance are distinguished by adding a subscript to the notation: linear compliance is denoted by f_{l} and nonlinear end-compliance by f_{nl}.

End-compliance is the simplest extension of minimum compliance to the geometric nonlinear range. The objective function, however, only considers the equilibrium point corresponding to the applied load and does not contain any information on the load-displacement path for lower load levels. In compliant structures this might lead to degeneracy of the design [15]. Minimization of complementary work could be considered in order to account for the complete load-displacement path from unloaded up to the final applied load. However, evaluating the complementary work and performing the sensitivity analysis for this objective function is computationally much more expensive. Klarbring and Strömberg [33] proposed to minimize the negative of the potential energy which has the important benefit that it does not require any adjoint equations to be solved in the sensitivity analysis. Note that end-compliance, complementary work and the negative of the potential energy are all equivalent measures of structural stiffness in case of a linear model.

The nonlinear equilibrium equations are written as:

$$\mathbf{g}_{\mathrm{nl}}\left(\boldsymbol{\rho}, \mathbf{u}\right) = \mathbf{R}\left(\boldsymbol{\rho}, \mathbf{u}\right) - \mathbf{P} = \mathbf{0} \tag{7}$$

The internal force vector $\mathbf{R}$ is expressed as the following integral over the reference configuration of the domain:

$$\mathbf{R}\left(\boldsymbol{\rho}, \mathbf{u}\right) = \sum_{e=1}^{n_{\mathrm{e}}} \int_{\Omega_e} \mathbf{B}^{\mathsf{T}}(\mathbf{u}) \mathbf{S}_e(\boldsymbol{\rho}, \mathbf{u}) \, \mathrm{d}\Omega \tag{8}$$

where $\mathbf{B}$ is the strain increment matrix and $\mathbf{S}_e$ is the vector of second Piola-Kirchhoff stresses. More detailed information on this formulation is found in standard textbooks on nonlinear finite element analysis [30, 31, 32]. In this paper the material behavior is described by means of the Saint Venant-Kirchhoff constitutive model which is a generalization of Hooke's law for small strain problems and which is expressed as:

$$\mathbf{S}_e(\boldsymbol{\rho}, \mathbf{u}) = E_e(\boldsymbol{\rho}) \mathbf{C}^0 \mathbf{E}(\mathbf{u}) \tag{9}$$

where $\mathbf{E}$ is the Green-Lagrange strain vector. The elastic constitutive matrix for unit-stiffness $\mathbf{C}^0$ is multiplied by the element's Young's modulus E_e which is again determined as a function of the design variables $\boldsymbol{\rho}$ through the SIMP relation (2) and the projection filter (3)–(4). It is well known that the simple linear constitutive relation (9) is not appropriate for describing large deformations, especially in the compressive range [31]. However, the applications in this paper only consider structures that undergo large displacements and small deformations for which the Saint Venant-Kirchhoff model is deemed sufficiently accurate. The present method can be modified in order to incorporate more advanced material laws such as Neo-Hookean models in case large deformation effects are important.

Equation (7) is solved by means of the Newton-Raphson method during the design optimization, i.e. the nonlinear displacements for a particular design $\boldsymbol{\rho}$ are determined iteratively by solving a number of local linearizations of the nonlinear system (7):

$$\mathbf{K_T}(\boldsymbol{\rho}, \mathbf{u}^{(k)})\Delta\mathbf{u}^{(k)} = -\mathbf{g}_{\mathrm{nl}}(\boldsymbol{\rho}, \mathbf{u}^{(k)}) \tag{10}$$

where $\Delta\mathbf{u}^{(k)} = \mathbf{u}^{(k+1)} - \mathbf{u}^{(k)}$ is the displacement increment and the tangent stiffness matrix $\mathbf{K_T}$ is defined as the Jacobian of $\mathbf{R}$:

$$\mathbf{K_T}(\boldsymbol{\rho}, \mathbf{u}) = \frac{\partial \mathbf{R}(\boldsymbol{\rho}, \mathbf{u})}{\partial \mathbf{u}} \tag{11}$$

There are a number of complications when geometric nonlinearity is accounted for in topology optimization [15, 34]. One well-known issue is the occurrence of artificial instabilities in the void phase of the design domain which affect the convergence of the Newton-Raphson solver. Several strategies for solving this problem have been presented in the literature including modified material interpolation schemes [35], an element removal strategy [34] and the element connectivity parameterization method [36]. However, these instabilities mainly occur in structures that undergo very large displacements such as compliant mechanisms. These types of applications are not of direct interest in this paper and therefore a simple convergence relaxation strategy as presented by Buhl et al. [15] is adopted here. In the following applications it was seen that the near-singularity (or small stiffness) of the void elements also complicates the numerical computation of nonlinear critical modes. A nonlinear critical point corresponds to an equilibrium state $\mathbf{u}_{\mathrm{c}}$ where the tangent stiffness matrix turns singular:

$$\mathbf{K_T}(\boldsymbol{\rho}, \mathbf{u}_{\mathrm{c}})\boldsymbol{\phi}_{\mathrm{c}} = \mathbf{0} \tag{12}$$

where $\boldsymbol{\phi}_{\mathrm{c}}$ is the nonlinear critical mode.

Although this paper only considers minimum end-compliance for the optimization of geometric nonlinear structures and also the robust algorithm presented in the following does not require the computation of critical points, a stability analysis also provides insight in the imperfection sensitivity of the optimized design. It was often seen that computing the lowest eigenpairs in the vicinity of a critical point of the structure results in non-informative artificial modes in the void phase.

Similar problems with artificial modes occur in the computation of linear buckling loads and eigenfrequencies in topology optimization [18, 37]. Artificial modes in linear buckling analysis are removed by using different stiffness interpolations for the constitutive stiffness matrix and the stress stiffness matrix. In applications of topology optimization for dynamic problems, spurious modes are removed by means of a modified mass interpolation which increases the local Rayleigh coefficient of the void region [38]. In this work, the modified interpolation strategy for dynamics is extended to the nonlinear mechanical setting in order to compute the critical points of the structure in a design domain. Rather than solving the eigenvalue problem (12) directly, artificial nonlinear buckling modes are removed by computing dynamic critical modes:

$$\left(\mathbf{K_T}(\boldsymbol{\rho}, \mathbf{u}_{\mathrm{c}}) - \omega^2 \mathbf{M}(\boldsymbol{\rho})\right) \boldsymbol{\phi}_{\mathrm{c}} = \mathbf{0} \tag{13}$$

where $\mathbf{M}$ is a suitable positive semi-definite mass matrix. When computing the nonlinear critical modes in a post-processing step of a 0/1 design, a mass interpolation $\mathbf{M}_e = \bar{\rho}_e^p \mathbf{M}_0$ can be employed. Alternatively, an element removal strategy [34] can likewise be used to compute the structural nonlinear buckling modes of a 0/1 design.

In the following applications, critical points are determined in the nonlinear analysis of the optimized structure by first traversing the equilibrium path using an arc-length algorithm with an orthogonal hyperplane constraint [30]. During this procedure the positive definiteness of the tangent stiffness matrix is tracked by checking the signs of the pivots of the matrix factorization. Whenever the definiteness of the tangent stiffness matrix changes and hence a critical point is passed, a local bi-section algorithm is initiated in order to accurately determine the critical load level [39]. The critical mode corresponding to this critical point is computed by means of Eq. (13).

2.3. Shallow arch

The design of a shallow arch is considered as a first application. The design domain and boundary conditions for the shallow arch are shown in Figure 1a. The design domain, which spans an angle $\alpha = 30°$ with an inner radius $R_{\text{in}} = 100$ m, outer radius $R_{\text{out}} = 104$ m and out-of-plane thickness $t = 1$ cm, is discretized by 800×60 finite elements. The material properties are a Young's modulus $E_0 = 200$ GPa and a Poisson's ratio $\nu = 0.3$. A small stiffness $E_{\text{min}} = 10^{-9}E_0$ is attributed to the void phase. The geometric complexity of the design is limited by means of the projection filter (3)–(4) with a filter radius $R = 0.25$ m, a projection threshold $\eta = 0$ for a minimum length scale in the material phase, and a maximum steepness $\beta = 32$. As is common in topology optimization of geometric nonlinear problems [15], a continuation scheme is used for the penalization parameter p in the SIMP law (2). When a Heaviside projection filter with a threshold $\eta = 0$ is used, the optimized design might contain bars consisting of intermediate densities and with radii smaller than the minimum length scale. The maximum penalization is therefore set to $p = 8$ in order to ensure convergence to nearly discrete designs with the current filter specifications. The design is optimized

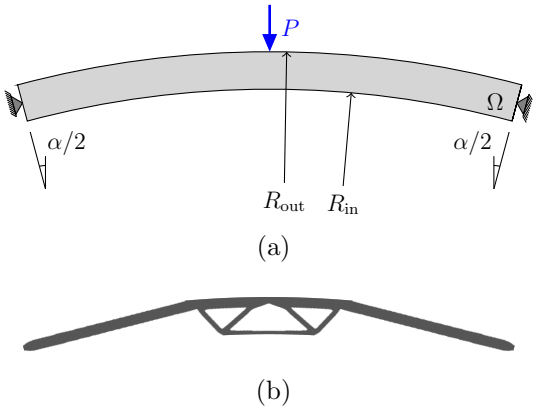

Figure 1: Topology optimization of a shallow arch: (a) design domain and boundary conditions, and (b) optimized nominal design.

for minimum end-compliance with a load $P = 800$ kN and the volume fraction of the design is limited to $V_{\text{max}} = 30$ %. The optimized design is shown in Figure 1b.

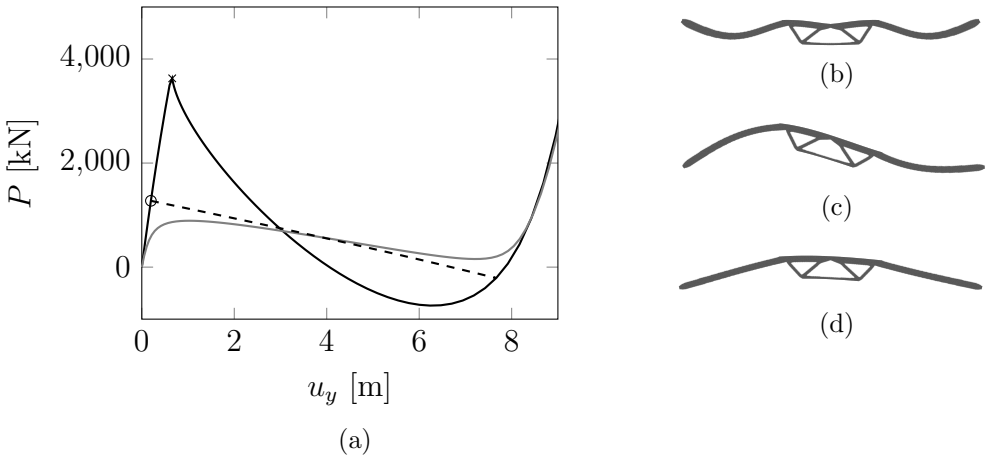

Figure 2: Nonlinear analysis of the nominal arch design: (a) load-displacement curve of the nominal design: the primary path (black line) of the perfect nominal design contains a limit point (cross) and unstable bifurcation point (circle) with bifurcation path (dashed black line). The limit point corresponds to the snap-through depicted in Figure (b) and the bifurcation point to the asymmetrical bifurcation mode in Figure (c). The load-displacement curve (gray line) of the imperfect design in Figure (d) is also shown.

The nonlinear analysis of the design is illustrated in Figure 2a where the load-displacement curve for the center of the arch at the location of the point load is shown. On the primary equilibrium path, the structural response is initially almost linear until a limit point is reached at $P = 3628$ kN corresponding to snap-through of the arch (Fig. 2b). The limit point clearly occurs at a much larger load level than the design load considered in the optimization and so it poses no direct harm for the stability of the design. However, the load-displacement curve of the nominal design also shows an unstable bifurcation point at a much smaller load $P = 1275$ kN as indicated by the dashed line in Figure 2a. The corresponding nonlinear bifurcation mode (Fig. 2c) is characterized by asymmetric buckling of the outer beams. The stability analysis of the design also reveals that the design is particularly sensitive to asymmetric imperfections associated with the unstable bifurcation, even at load levels well below the critical load level. This is illustrated by considering a slightly imperfect design (Fig. 2d). The load-displacement curve for this imperfect version is shown as the gray line in Figure 2a: the displacements are much larger and the response is clearly nonlinear at load levels far below the critical load.

2.4. Pinned column

This application examines the design of a slender column. The design domain for the pinned column (Fig. 3a) has a height $H = 3$ m and an out-of-plane thickness $t = 0.01$ m. The domain is discretized using a finite element mesh with 288×96 square plane elements. The material properties are again a Poisson's ratio $\eta = 0.3$ and Young's moduli $E_0 = 200$ GPa and $E_{\min} = 10^{-9}E_0$. A maximum penalization $p = 3$ is used in the SIMP law (2). A projection filter with filter radius $R = 0.0167H$, a projection threshold $\eta = 0.5$ and a maximum value for the steepness $\beta = 32$ is employed. The design is optimized for minimum end-compliance with an allowed volume fraction $V_{\max} = 0.2$. The vertical load is $P = 877$ kN, which corresponds to approximately 60 % of the Euler buckling load $P_c = 1462$ kN for a perfectly straight pinned bar with uniform cross section $t \times V_{\max}H/3$ and height H.

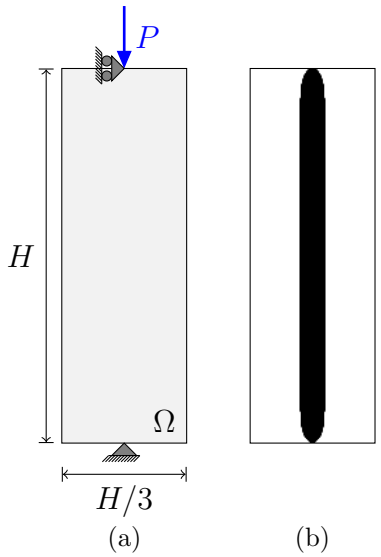

Figure 3: Pinned column: (a) design domain and boundary conditions, (b) nominal design.

As expected, the optimized design (Fig. 3b) corresponds to a straight column with a (nearly) uniform cross section. The load-displacement curve for the vertical displacement of the top of the column is shown in Figure 4a. The design shows the typical behavior of a pinned column: the response of the perfect design is linear until a stable bifurcation point is reached at $P = 1617$ kN (note that the buckling load is slightly larger than the theoret-

ical Euler buckling load P_c due to the non-uniform section of the optimized design). Figure 4a also shows the linear and nonlinear response of an imperfect design (Fig. 4b). It can be seen that the contribution of geometric nonlinear effects (i.e. the difference between linear and nonlinear response) increases strongly with the load level. The response of the imperfect design becomes highly nonlinear as the load approaches the buckling load of the perfect design.

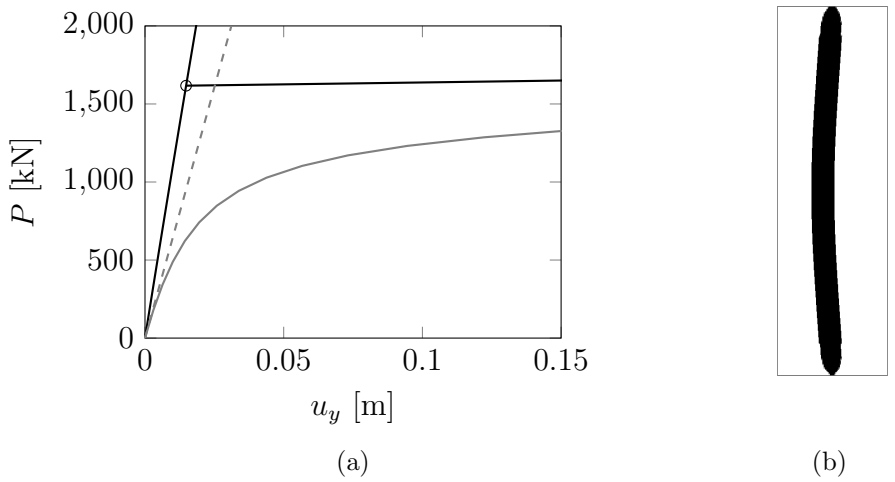

Figure 4: Pinned column: load-displacement path of the nominal design: equilibrium path for the perfect design (black line) with bifurcation point (circle). Equilibrium paths of the imperfect design in Fig. (b): linear small displacement response (gray dashed line) and nonlinear response (gray line).

3. Robust optimization

3.1. Geometric imperfections

This paper adopts a probabilistic framework for robust optimization where uncertainties are modeled as random variables characterized by a probability distribution. Random variables are defined as functions of the elementary event θ of the event space Θ. Geometric imperfections are modeled using a Lagrangian approach in this paper. A random field of imperfections $\mathbf{p} : \Omega \times \Theta \to \mathbb{R}^n$ is added to the material coordinates $\mathbf{x}$ of the design domain:

$$\tilde{\mathbf{x}}(\mathbf{x}, \theta) = \mathbf{x} + \mathbf{p}(\mathbf{x}, \theta) \tag{14}$$

where $\tilde{\mathbf{x}}(\mathbf{x}, \theta)$ are the uncertain material coordinates of the imperfect design. In a discretized finite element setting, this Lagrangian approach corresponds to shifting the nodes in the finite element mesh. It is important to note that in this paper the imperfections are assumed to be sufficiently small such that they do not cause any strong distortions of the finite element mesh. An Eulerian approach [11, 12, 40] should be adopted to model the imperfections in case this assumption can not be made.

It is assumed that the imperfections $\mathbf{p}(\mathbf{x}, \theta)$ can be modeled as a zero-mean Gaussian random field. A Gaussian random field is fully characterized by its mean function $\mathbf{m}_\mathbf{p}(\mathbf{x})$ and covariance function $\mathbf{C}_\mathbf{p}(\mathbf{x}, \mathbf{x}')$:

$$\mathbf{m}_\mathbf{p}(\mathbf{x}) = \mathbb{E}\left[\mathbf{p}(\mathbf{x}, \theta)\right] = \mathbf{0} \tag{15}$$

$$\begin{aligned} \mathbf{C}_\mathbf{p}(\mathbf{x}, \mathbf{x}') &= \mathrm{Cov}\left[\mathbf{p}(\mathbf{x}, \theta), \mathbf{p}(\mathbf{x}', \theta)\right] \\ &= \mathbb{E}\left[\left(\mathbf{p}(\mathbf{x}, \theta) - \mathbf{m}_\mathbf{p}(\mathbf{x})\right)\left(\mathbf{p}(\mathbf{x}', \theta) - \mathbf{m}_\mathbf{p}(\mathbf{x}')\right)^\mathsf{T}\right] \end{aligned} \tag{16}$$

where $\mathbb{E}$ is the expectation operator. The horizontal and vertical components of the random field $\mathbf{p}(\mathbf{x}, \theta)$ are assumed to be uncorrelated in the present study which enables the following representation of the covariance function in two dimensional problems:

$$\mathbf{C}_\mathbf{p}(\mathbf{x}, \mathbf{x}') = \begin{bmatrix} C_{p_1}(\mathbf{x}, \mathbf{x}') & 0 \\ 0 & C_{p_2}(\mathbf{x}, \mathbf{x}') \end{bmatrix} \tag{17}$$

A squared exponential covariance function is used for the covariance function C_{p_i} of component p_i of the random vector:

$$C_{p_i}(\mathbf{x}, \mathbf{x}') = \sigma_{p_i}^2 \exp\left[-\left(\left(\frac{x - x'}{l_{\mathrm{c}x}}\right)^2 + \left(\frac{y - y'}{l_{\mathrm{c}y}}\right)^2\right)\right] \tag{18}$$

where σ_{p_i} is the standard deviation of the component p_i of the random field and $l_{\mathrm{c}x}$ and $l_{\mathrm{c}y}$ are the correlation lengths of the random field in the coordinate directions x and y.

It is assumed that the structure is placed correctly on the supports, i.e., geometric imperfections are zero at the location of the supports. These constraints can be incorporated in the description of the random field by means of a conditional random field [41, 42]. The conditional distribution of a Gaussian random field given some known values in a set of points $\{\bar{\mathbf{x}}_i \in \Omega | i \in 1, \ldots, m\}$ is also Gaussian with a modified mean and covariance function. Since the

imposed value of zero already corresponds to the mean value, only the covariance function has to be replaced by the conditional covariance function $\tilde{\mathbf{C}}_{\mathbf{p}}(\mathbf{x}, \mathbf{x}')$ which is expressed as:

$$\begin{aligned}\tilde{\mathbf{C}}_{\mathbf{p}}(\mathbf{x}, \mathbf{x}') &= \mathrm{Cov}\left[\mathbf{p}(\mathbf{x}, \theta), \mathbf{p}(\mathbf{x}', \theta) | \mathbf{p}(\bar{\mathbf{x}}_i, \theta) = \mathbf{0}\right] \\ &= \mathbf{C}_{\mathbf{p}}(\mathbf{x}, \mathbf{x}') - \mathbf{C}_{\mathbf{p}\bar{\mathbf{p}}}^{\mathsf{T}}(\mathbf{x}) \mathbf{C}_{\bar{\mathbf{p}}\bar{\mathbf{p}}}^{-1} \mathbf{C}_{\mathbf{p}\bar{\mathbf{p}}}(\mathbf{x}')\end{aligned} \tag{19}$$

where $\mathbf{C}_{\mathbf{p}\bar{\mathbf{p}}}(\mathbf{x})$ is the covariance function of $\mathbf{p}(\mathbf{x})$ and $\mathbf{p}(\bar{\mathbf{x}}_i)$, and $\mathbf{C}_{\bar{\mathbf{p}}\bar{\mathbf{p}}}$ is the covariance matrix of $\mathbf{p}(\bar{\mathbf{x}}_i)$.

A discrete approximation of the Gaussian random field $\mathbf{p}(\mathbf{x}, \theta)$ is established by means of the Expansion Optimal Linear Estimation method (EOLE) by Li and Der Kiureghian [43]. In the EOLE method, the random field is initially only considered in a discrete number of points N in the domain Ω. The random vector corresponding to the values of the random field in these points is a multivariate Gaussian random vector which is decorrelated by means of principal component analysis. At intermediate locations, the random field is approximated by means of the Optimal Linear Estimator (OLE) method. The resulting EOLE expansion is written as a sum of deterministic mode functions $\boldsymbol{\varphi}_k(\mathbf{x})$ multiplied by standard Gaussian random variables $\xi_k(\theta)$. Equation (14) is approximated as:

$$\tilde{\mathbf{x}}(\mathbf{x}, \theta) \approx \mathbf{x} + \sum_{k=1}^{M} \boldsymbol{\varphi}_k(\mathbf{x}) \xi_k(\theta) \tag{20}$$

where $M \leq N$ is the number of modes included in the expansion. The number of modes required for an accurate approximation is typically determined based on the variance of the truncation error:

$$\begin{aligned}e_M^2(\mathbf{x}) &= \mathbb{E}\left[\left(\mathbf{p}(\mathbf{x}, \theta) - \sum_{k=1}^{M} \boldsymbol{\varphi}_k(\mathbf{x}) \xi_k(\theta)\right)^{\mathsf{T}} \left(\mathbf{p}(\mathbf{x}, \theta) - \sum_{k=1}^{M} \boldsymbol{\varphi}_k(\mathbf{x}) \xi_k(\theta)\right)\right] \\ &= \mathbb{E}\left[\mathbf{p}(\mathbf{x}, \theta)^{\mathsf{T}} \mathbf{p}(\mathbf{x}, \theta)\right] - \mathbb{E}\left[\left(\sum_{k=1}^{M} \boldsymbol{\varphi}_k(\mathbf{x}) \xi_k(\theta)\right)^{\mathsf{T}} \left(\sum_{k=1}^{M} \boldsymbol{\varphi}_k(\mathbf{x}) \xi_k(\theta)\right)\right] \\ &= \mathrm{Tr}\left(\mathbf{C}_{\mathbf{p}}(\mathbf{x}, \mathbf{x})\right) - \sum_{k=1}^{M} \boldsymbol{\varphi}_k(\mathbf{x})^{\mathsf{T}} \boldsymbol{\varphi}_k(\mathbf{x})\end{aligned} \tag{21}$$

where Tr is the matrix trace.

3.2. Robust optimization problem

The previous section showed how the geometric imperfections can be expressed in terms of a vector of i.i.d. standard Gaussian random variables $\boldsymbol{\xi}$. The uncertainty in the response of the imperfect structures can be characterized by incorporating the imperfections in the equilibrium equations (7):

$$\mathbf{g}(\boldsymbol{\rho}, \mathbf{u}, \boldsymbol{\xi}) = \mathbf{R}(\boldsymbol{\rho}, \mathbf{u}, \boldsymbol{\xi}) - \mathbf{P} = \mathbf{0} \tag{22}$$

Note that the external load vector $\mathbf{P}$ is assumed to be independent of the imperfections. The uncertain displacements $\mathbf{u}(\boldsymbol{\rho}, \boldsymbol{\xi})$ can be expressed as a function of the design variables $\boldsymbol{\rho}$ and random variables $\boldsymbol{\xi}$ by solving Equation (22). As a result, the performance is also uncertain and is denoted similarly by $f(\boldsymbol{\rho}, \boldsymbol{\xi})$. Several approaches are commonly distinguished in the literature for incorporating (probabilistic) uncertainties in optimization—see for example a number of review papers on robust optimization [44, 45]. For instance, in reliability-based design optimization (RBDO), a certain level of reliability with respect to failure (i.e. infeasibility) of the design is ensured by formulating the constraints in the optimization problem as chance constraints. However, this paper adopts a robust design optimization (RDO) strategy where uncertainties in the design performance are taken into account by defining the robust objective function f_{R} as a weighted sum of the mean m_f and standard deviation σ_f of the performance. The robust counterpart for the minimum (end-)compliance problem (5) is therefore expressed as follows:

$$\begin{aligned} \min_{\boldsymbol{\rho}} \;\; & f_{\mathrm{R}}(\boldsymbol{\rho}) = m_f(\boldsymbol{\rho}) + \omega \sigma_f(\boldsymbol{\rho}) \\ \text{s.t.} \;\; & V(\boldsymbol{\rho}) - V_{\max} \leq 0 \\ & \mathbf{0} \leq \boldsymbol{\rho} \leq \mathbf{1} \end{aligned} \tag{23}$$

where the mean m_f and standard deviation σ_f of the objective function are defined as:

$$m_f(\boldsymbol{\rho}) = \mathbb{E}\left[f(\boldsymbol{\rho}, \boldsymbol{\xi})\right] \tag{24}$$

$$\sigma_f(\boldsymbol{\rho}) = \sqrt{\mathrm{Var}\left[f(\boldsymbol{\rho}, \boldsymbol{\xi})\right]} = \sqrt{\mathbb{E}\left[\left(f(\boldsymbol{\rho}, \boldsymbol{\xi})\right)^2 - \left(m_f(\boldsymbol{\rho})\right)^2\right]} \tag{25}$$

The weighting parameter ω is chosen equal to 1 in this study.

3.3. Stochastic perturbation method

In order to solve the robust optimization problem (23), the stochastic moments m_f and σ_f (and their sensitivities) have to be estimated in each design iteration of the optimization algorithm. Various uncertainty quantification techniques can be applied for this purpose [46]. For example, numerical quadrature methods [7, 47] or simulation methods (e.g. the Monte Carlo method) [11] are often applied in robust topology optimization. These methods are generally applicable and simple to apply as they only require the evaluation of a number of independent deterministic function evaluations. However, a second-order perturbation method [48, 49] is adopted in this work in order to avoid having to perform multiple nonlinear finite element analyses in each design iteration.

The perturbation method approximates the function $f(\mathbf{u}(\boldsymbol{\xi}))$ by constructing a Taylor series, usually of first- or second-order, in the direction of the random variables $\boldsymbol{\xi}$. Note that the $\boldsymbol{\rho}$-dependence of the displacements and performance is dropped for notational convenience in the following (e.g. $\mathbf{u}(\boldsymbol{\rho}, \boldsymbol{\xi})$ is written as $\mathbf{u}(\boldsymbol{\xi})$), while the dependence of the performance on the displacements is included explicitly in $f(\mathbf{u}(\boldsymbol{\xi}))$. The Taylor expansion is established at the nominal design ($\boldsymbol{\xi} = \mathbf{0}$):

$$f(\mathbf{u}(\boldsymbol{\xi})) \approx f_0 + \sum_{i=1}^{M} f_{,i}\xi_i + \frac{1}{2}\sum_{i=1}^{M}\sum_{j=1}^{M} f_{,ij}\xi_i\xi_j \tag{26}$$

where:

$$f_0 = f(\mathbf{u}(\mathbf{0})) \qquad f_{,i} = \left.\frac{\mathrm{d}f}{\mathrm{d}\xi_i}\right|_{\boldsymbol{\xi}=\mathbf{0}} \qquad f_{,ij} = \left.\frac{\mathrm{d}^2 f}{\mathrm{d}\xi_i \mathrm{d}\xi_j}\right|_{\boldsymbol{\xi}=\mathbf{0}} \tag{27}$$

The computational cost of the perturbation method is governed by the effort related to the computation of the coefficients $(f_0, f_{,i}, f_{,ij})$. An efficient strategy based on adjoint differentiation is presented for this purpose further below.

Once the coefficients $(f_0, f_{,i}, f_{,ij})$ have been computed, the stochastic moments of the quadratic function (26) can be expressed in closed form and are

used as estimates for the mean and variance of the performance $f(\mathbf{u}(\boldsymbol{\xi}))$:

$$\mathbb{E}[f] \approx \mathbb{E}[f]_2 = f_0 + \sum_{i=1}^{M} f_{,i}\mathbb{E}[\xi_i] + \frac{1}{2}\sum_{i=1}^{M}\sum_{j=1}^{M} f_{,ij}\mathbb{E}[\xi_i\xi_j] \tag{28}$$

$$\mathrm{Var}[f] \approx \mathrm{Var}[f]_2 = \mathbb{E}\left[\left(f_0 + \sum_{i=1}^{M} f_{,i}\xi_i + \frac{1}{2}\sum_{i=1}^{M}\sum_{j=1}^{M} f_{,ij}\xi_i\xi_j - \mathbb{E}[f]_2\right)^2\right] \tag{29}$$

Since $\boldsymbol{\xi}$ is a vector of i.i.d. standard normal random variables, these expressions simplify to:

$$\mathbb{E}[f]_2 = f_0 + \frac{1}{2}\sum_{i=1}^{M} f_{,ii} \tag{30}$$

$$\mathrm{Var}[f]_2 = \sum_{i=1}^{M} f_{,i}^2 + \frac{1}{2}\sum_{i=1}^{M}\sum_{j=1}^{M} f_{,ij}f_{,ji} \tag{31}$$

Note that in the general case of non-Gaussian random variables additional terms related to higher-order stochastic moments appear in the expression for the variance [44].

The coefficients of the quadratic approximation (26) are computed using the chain rule of differentiation:

$$f_0 = f(\mathbf{u}_0) \tag{32}$$

$$f_{,i} = \frac{\partial f}{\partial \mathbf{u}}\mathbf{u}_{,i} \tag{33}$$

$$f_{,ij} = \mathbf{u}_{,i}^{\mathsf{T}}\frac{\partial^2 f}{\partial \mathbf{u}\partial \mathbf{u}}\mathbf{u}_{,j} + \frac{\partial f}{\partial \mathbf{u}}\mathbf{u}_{,ij} \tag{34}$$

where:

$$\mathbf{u}_0 = \mathbf{u}(\mathbf{0}) \qquad \mathbf{u}_{,i} = \left.\frac{\partial \mathbf{u}}{\partial \xi_i}\right|_{\boldsymbol{\xi}=\mathbf{0}} \qquad \mathbf{u}_{,ij} = \left.\frac{\partial^2 \mathbf{u}}{\partial \xi_i \partial \xi_j}\right|_{\boldsymbol{\xi}=\mathbf{0}} \tag{35}$$

The variables $(\mathbf{u}_0, \mathbf{u}_{,i}, \mathbf{u}_{,ij})$ are found by differentiation of the nonlinear equi-

librium equations (22) in the direction of the random variables:

$$\mathbf{g}_0(\mathbf{u}_0) = \mathbf{R}(\mathbf{u}_0, \mathbf{0}) - \mathbf{P} = \mathbf{0} \tag{36}$$

$$\mathbf{g}_{,i}(\mathbf{u}_0, \mathbf{u}_{,i}) = \mathbf{K_{T0}}\mathbf{u}_{,i} + \frac{\partial \mathbf{R}}{\partial \xi_i} = \mathbf{0} \qquad i = 1, \ldots, M \tag{37}$$

$$\begin{aligned}\mathbf{g}_{,ij}(\mathbf{u}_0, \mathbf{u}_{,i}, \mathbf{u}_{,j}, \mathbf{u}_{,ij}) = &\mathbf{K_{T0}}\mathbf{u}_{,ij} + \frac{\partial \mathbf{K_T}}{\partial \xi_i}\mathbf{u}_{,j} + \frac{\partial \mathbf{K_T}}{\partial \xi_j}\mathbf{u}_{,i} \\ &+ \frac{\partial^2 \mathbf{R}}{\partial \xi_i \partial \xi_j} + \left(\frac{\partial \mathbf{K_T}}{\partial \mathbf{u}}\mathbf{u}_{,i}\right)\mathbf{u}_{,j} = \mathbf{0} \quad i, j = 1, \ldots, M\end{aligned} \tag{38}$$

The derivatives of the internal force vector and tangent stiffness matrix such as $\partial \mathbf{R}/\partial \xi_i$ and $\partial \mathbf{K_T}/\partial \xi_i$ correspond to shape variations of the finite element mesh. The computation of these terms is obviously more involved than, e.g., for variable material properties, due to the rather complicated nonlinear dependence of the finite element matrices on the nodal coordinates. A semi-analytical approach, known from shape optimization [50, 51], is used in this paper in order to avoid the tedious derivation of analytical expressions. Instead, the derivatives of the finite element matrices are computed by means of finite differences. The directional derivatives of $\mathbf{K_T}$ with respect to the displacements are also evaluated most easily using finite differences.

The system of equations (36)–(38) should be solved sequentially. The first equation (36) corresponds to the state equation of the nominal system, while the equations (37)–(38) are both linear in the unknowns $\mathbf{u}_{,i}$ and $\mathbf{u}_{,ij}$ with the same coefficient matrix, i.e. the tangent stiffness matrix $\mathbf{K_{T0}} = \partial \mathbf{R}(\mathbf{u}_0, \mathbf{0})/\partial \mathbf{u}$. The perturbation method, therefore, only requires a single factorization of the nominal stiffness matrix $\mathbf{K_{T0}}$ in order to solve the linear system (37)–(38) with $M + M^2$ right-hand sides (and actually $(3M + M^2)/2$ if symmetry of $\mathbf{u}_{,ij}$ is considered). Hence the increase of the computational cost is proportional to a number of $M + M^2$ right-hand side vector assemblies and forward and back substitutions of the factorized stiffness matrix. This strategy for computing the perturbation coefficients is equivalent to direct differentiation [28] since all imperfection sensitivities of the displacement vector are first computed before being utilized in the computation of the sensitivities of the objective function.

When the aim is to quantify the uncertainty of a single output function f, the computational effort of the perturbation method can be further reduced by following an adjoint approach to differentiation. In particular for a second-

order Taylor expansion with the coefficients (32)–(34) and the corresponding set of state equations (36)–(38), an adjoint formulation is derived by solving Eq. (38) for $\mathbf{u}_{,ij}$ and implementing the resulting expression into the second-order derivatives $f_{,ij}$:

$$\begin{aligned} f_{,ij} &= \mathbf{u}_{,i}^{\mathsf{T}} \frac{\partial^2 f}{\partial \mathbf{u} \partial \mathbf{u}} \mathbf{u}_{,j} - \frac{\partial f}{\partial \mathbf{u}} \mathbf{K}_{\mathbf{T}0}^{-1} \left(\frac{\partial \mathbf{K}_{\mathbf{T}}}{\partial \xi_i} \mathbf{u}_{,j} + \frac{\partial \mathbf{K}_{\mathbf{T}}}{\partial \xi_j} \mathbf{u}_{,i} + \frac{\partial^2 \mathbf{R}}{\partial \xi_i \partial \xi_j} + \left(\frac{\partial \mathbf{K}_{\mathbf{T}}}{\partial \mathbf{u}} \mathbf{u}_{,i} \right) \mathbf{u}_{,j} \right) \\ &= \mathbf{u}_{,i}^{\mathsf{T}} \frac{\partial^2 f}{\partial \mathbf{u} \partial \mathbf{u}} \mathbf{u}_{,j} - \mathbf{v}^{\mathsf{T}} \left(\frac{\partial \mathbf{K}_{\mathbf{T}}}{\partial \xi_i} \mathbf{u}_{,j} + \frac{\partial \mathbf{K}_{\mathbf{T}}}{\partial \xi_j} \mathbf{u}_{,i} + \frac{\partial^2 \mathbf{R}}{\partial \xi_i \partial \xi_j} + \left(\frac{\partial \mathbf{K}_{\mathbf{T}}}{\partial \mathbf{u}} \mathbf{u}_{,i} \right) \mathbf{u}_{,j} \right) \end{aligned} \tag{39}$$

where the adjoint variable $\mathbf{v}$ is defined as the solution of the following linear system:

$$\mathbf{g}_{\mathrm{a}}(\mathbf{u}_0, \mathbf{v}) = \mathbf{K}_{\mathbf{T}0}^{\mathsf{T}} \mathbf{v} - \left(\frac{\partial f}{\partial \mathbf{u}} \right)^{\mathsf{T}} = \mathbf{0} \tag{40}$$

As a result, the second-order derivatives $f_{,ij}(\mathbf{u}_0, \mathbf{u}_{,i}, \mathbf{v})$ are expressed in terms of the variables $(\mathbf{u}_0, \mathbf{u}_{,i}, \mathbf{v})$ and it is no longer necessary to compute the second-order perturbations $\mathbf{u}_{,ij}$. Since $\mathbf{v}$ represents a single unknown vector, the set of variables $(\mathbf{u}_0, \mathbf{u}_{,i}, \mathbf{v})$ and the corresponding set of equations (36)–(37) and (40) grow linearly rather than quadratically with the number M of random variables.

A similar linear growth can be achieved in the design sensitivity analysis by directly computing the sensitivities of the robust objective $f_{\mathrm{R}}(\mathbf{u}_0, \mathbf{u}_{,i}, \mathbf{v})$ which aggregates all the imperfection sensitivities $(f_0, f_{,i}, f_{,ij})$. The design sensitivities and adjoint equations are derived by introducing the Lagrangian:

$$\hat{f}_{\mathrm{R}}(\mathbf{u}_0, \mathbf{u}_{,i}, \mathbf{v}, \boldsymbol{\lambda}_0, \boldsymbol{\lambda}_i, \boldsymbol{\gamma}) = f_{\mathrm{R}}(\mathbf{u}_0, \mathbf{u}_{,i}, \mathbf{v}) - \boldsymbol{\lambda}_0^{\mathsf{T}} \mathbf{g}_0(\mathbf{u}_0) - \sum_{i=1}^{M} \boldsymbol{\lambda}_i^{\mathsf{T}} \mathbf{g}_{,i}(\mathbf{u}, \mathbf{u}_{,i}) - \boldsymbol{\gamma}^{\mathsf{T}} \mathbf{g}_{\mathrm{a}}(\mathbf{u}_0, \mathbf{v}) \tag{41}$$

Setting the partial derivatives with respect to the state variables $(\mathbf{u}_0, \mathbf{u}_{,i}, \mathbf{v})$

equal to zero leads to the following set of adjoint systems:

$$\mathbf{K}_{\mathbf{T}0}\boldsymbol{\gamma} = \left(\frac{\partial f_{\mathrm{R}}}{\partial \mathbf{v}}\right)^{\mathsf{T}} \tag{42}$$

$$\mathbf{K}_{\mathbf{T}0}^{\mathsf{T}}\boldsymbol{\lambda}_i = \left(\frac{\partial f_{\mathrm{R}}}{\partial \mathbf{u}_{,i}}\right)^{\mathsf{T}} \qquad i = 1, \ldots, M \tag{43}$$

$$\mathbf{K}_{\mathbf{T}0}^{\mathsf{T}}\boldsymbol{\lambda}_0 = \left(\frac{\partial f_{\mathrm{R}}}{\partial \mathbf{u}_0}\right)^{\mathsf{T}} - \sum_{i=1}^{M}\left(\frac{\mathrm{d}\mathbf{K}_{\mathbf{T}}}{\mathrm{d}\xi_i}\right)^{\mathsf{T}}\boldsymbol{\lambda}_i - \left(\frac{\partial \mathbf{K}_{\mathbf{T}}}{\partial \mathbf{u}}\mathbf{v}\right)^{\mathsf{T}}\boldsymbol{\gamma} \tag{44}$$

where the derivatives of $\mathbf{K}_{\mathbf{T}}$ are understood as:

$$\frac{\mathrm{d}\mathbf{K}_{\mathbf{T}}}{\mathrm{d}\xi_i} = \frac{\partial \mathbf{K}_{\mathbf{T}}}{\partial \mathbf{u}}\mathbf{u}_{,i} + \frac{\partial \mathbf{K}_{\mathbf{T}}}{\partial \xi_i} \tag{45}$$

The design sensitivities of f_{R} correspond to the partial derivatives of the Lagrangian (41) with respect to the design variables:

$$\frac{\mathrm{d}f_{\mathrm{R}}}{\mathrm{d}\boldsymbol{\rho}} = \frac{\partial \hat{f}_{\mathrm{R}}}{\partial \boldsymbol{\rho}} = \frac{\partial f_{\mathrm{R}}}{\partial \boldsymbol{\rho}} - \boldsymbol{\lambda}_0^{\mathsf{T}}\frac{\partial \mathbf{g}_0}{\partial \boldsymbol{\rho}} - \sum_{i=1}^{M}\boldsymbol{\lambda}_i^{\mathsf{T}}\frac{\partial \mathbf{g}_{,i}}{\partial \boldsymbol{\rho}} - \boldsymbol{\gamma}^{\mathsf{T}}\frac{\partial \mathbf{g}_{\mathrm{a}}}{\partial \boldsymbol{\rho}} \tag{46}$$

It should be noted that although no direct dependence of the performance function $f(\mathbf{u}(\boldsymbol{\rho}, \boldsymbol{\xi}))$ on the design is considered (e.g. for compliance $f = \mathbf{P}^{\mathsf{T}}\mathbf{u}(\boldsymbol{\rho}, \boldsymbol{\xi})$ there is only an indirect dependence through the design dependent displacements), $\partial f_{\mathrm{R}}/\partial \boldsymbol{\rho}$ is not zero since $f_{,ij}$ is expanded using Eq. (39) in the adjoint approach. In summary, the adjoint approach involves $2 + 2M$ additional right-hand sides in the linear system with coefficient matrix $\mathbf{K}_{\mathbf{T}0}$ compared to a deterministic function evaluation and sensitivity analysis. The quadratic perturbation method is therefore particularly efficient for problems with a small number M of random variables.

3.4. Shallow arch

The imperfections in the shallow arch are modeled as an isotropic random field. The horizontal and vertical components are initially described by stationary random fields $p_i(\mathbf{x}, \theta)$ with squared exponential covariance function (18) with $\sigma_{p_i} = 0.33$ m and $l_{cx} = l_{cy} = 17.45$ m. The random field is conditioned to have zero imperfections at the supports using Eq. (19). The variance of the conditioned random field is shown in Figure 5a which illustrates that the imperfections are small close to the supports and increase

towards the center of the design domain. A truncated EOLE expansion with three modes for each component p_i is sufficiently accurate as the variance of the error remains below 2.5 % of the variance of the imperfections (Fig. 5b). In total, there are $M = 6$ EOLE modes which are illustrated in Figure 6.

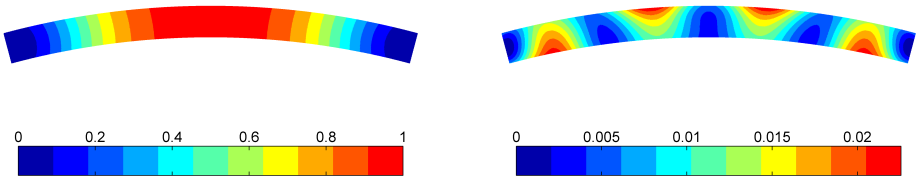

(a) (b)

Figure 5: Random field of imperfections for the shallow arch: (a) Normalized variation $C_{p_i}(\mathbf{x},\mathbf{x})/\sigma^2_{p_i}$ of the conditional random field; (b) Normalized error $e^2_M(\mathbf{x})/(2\sigma^2_{p_i})$ of the EOLE expansion.

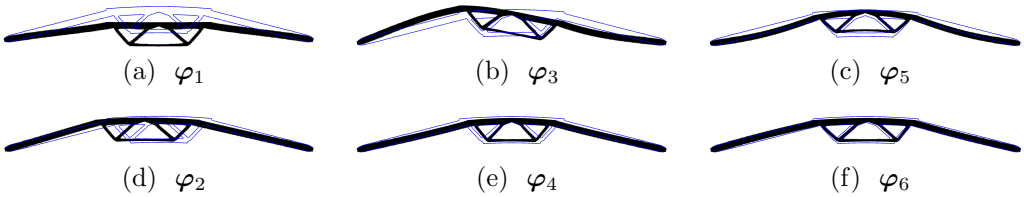

(a) φ_1 (b) φ_3 (c) φ_5

(d) φ_2 (e) φ_4 (f) φ_6

Figure 6: First six EOLE modes of the random field $\mathbf{p}(\mathbf{x},\theta)$ applied to the nominal arch design.

Figure 7: Robust design for the shallow arch.

The design obtained by using the robust approach outlined in the previous sections is shown in Figure 7: the design is clearly more robust and it can be anticipated that the critical load of asymmetric buckling is larger due to the reduced slenderness of the outer beams. The performance of the designs is assessed by an elaborate Monte Carlo simulation with 10 000 samples.

The results of the different designs are compared in Table 1. It can be seen that the nominal design is very sensitive to imperfections as indicated by the large mean $m_{f_{\mathrm{nl}}}$ and standard deviation $\sigma_{f_{\mathrm{nl}}}$ of the nonlinear end-compliance. The sensitivity of the nominal design can be mainly attributed to geometric nonlinear effects related to the unstable bifurcation since the linear statistics $m_{f_{\mathrm{l}}}$ and $\sigma_{f_{\mathrm{l}}}$ of the nominal design are much smaller (and in fact quite similar to those of the robust design). Although the nominal performance f_{nl} of the robust design is slightly worse than for the nominal design, the robust design is much less sensitive to geometric imperfections as the statistics $m_{f_{\mathrm{nl}}}$ and $\sigma_{f_{\mathrm{nl}}}$ are much smaller. Furthermore, the minor differences between linear and nonlinear statistics of the robust design suggest that the imperfections no longer trigger any significant geometric nonlinear behavior in the design.

In order to further illustrate the effect of robust optimization, Figure 8 compares the nonlinear end-compliance of the nominal and robust design as a function of the third EOLE mode (the third mode resembles the asymmetric buckling mode and is therefore expected to have a particularly large influence on the structural performance). It can be seen that the nominal performance of the robust design (i.e. at $\xi_3 = 0$) is slightly worse, but the performance of the design is much less affected by geometric imperfections. Finally, it should be noted that the second-order perturbation method proves to be very accurate in the present robust optimization as indicated by the small difference between the estimates $\hat{m}_{f_{\mathrm{nl}}}$ and $\hat{\sigma}_{f_{\mathrm{nl}}}$ and the statistics $m_{f_{\mathrm{nl}}}$ and $\sigma_{f_{\mathrm{nl}}}$ in Table 1. Furthermore, in Figure 8, the quadratic approximation is almost indistinguishable from the actual performance of the robust design. The quadratic approximation for the nominal design (Fig. 8) is less accurate which is to be expected as (geometric) nonlinearity is more pronounced in this design.

Design	f_{nl}	$m_{f_{\mathrm{l}}}$	$\sigma_{f_{\mathrm{l}}}$	$\hat{m}_{f_{\mathrm{nl}}}$	$\hat{\sigma}_{f_{\mathrm{nl}}}$	$m_{f_{\mathrm{nl}}}$	$\sigma_{f_{\mathrm{nl}}}$	f_{Rnl}
Nominal	97.1	108.1	20.1	/	/	337.3	1033.3	1370.6
Robust	121.1	119.1	11.5	126.3	12.1	126.6	13.1	139.7

Table 1: Results for the optimized shallow arch designs including the nominal nonlinear performance f_{nl}, the mean $m_{f_{\mathrm{l}}}$ and standard deviation $\sigma_{f_{\mathrm{l}}}$ of the linear compliance obtained by a Monte Carlo simulation with 10 000 samples, the estimated statistics at the end of the robust optimization $\hat{m}_{f_{\mathrm{nl}}}$ and $\hat{\sigma}_{f_{\mathrm{nl}}}$, the mean $m_{f_{\mathrm{nl}}}$ and standard deviation $\sigma_{f_{\mathrm{nl}}}$ of the nonlinear end-compliance, and the robust objective $f_{\mathrm{Rnl}} = m_{f_{\mathrm{nl}}} + \sigma_{f_{\mathrm{nl}}}$. All results are in kJ.

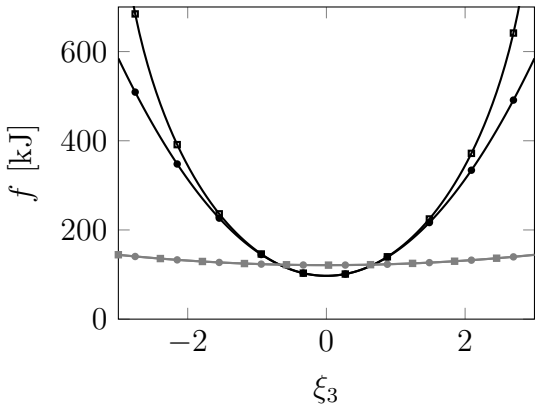

Figure 8: Shallow arch: nonlinear end-compliance of the nominal design (black squared line) and the robust design (gray squared line) as a function of the third mode of imperfection $\boldsymbol{\varphi}_3$; quadratic approximations by the second-order perturbation method for the nominal design (black circled line) and robust design (gray circled line).

3.5. Pinned column

The column is only perturbed by horizontal imperfections, i.e. the vertical component $p_2 = 0$. The horizontal component is modeled by a zero-mean Gaussian random field $p_1(\mathbf{x}, \theta)$ with covariance function (18) and the following parameters: $\sigma_{p_1} = 0.0208H$, $l_{cx} = \infty$ and $l_{cy} = H/2$. Furthermore, the imperfections are set equal to zero at the bottom and top support using the conditional random field formulation (19). Based on the mean square error after truncation an EOLE expansion with $M = 3$ modes is sufficiently accurate.

The robust design obtained using the perturbation method is shown in Figure 9. It can be seen that the sensitivity with respect to imperfections is reduced by an increase in bending stiffness at the cost of the compressive stiffness which is slightly reduced.

The performance of the designs is compared in Table 2. Similar conclusions as in the previous example can be drawn: the robust design has a slightly worse nominal performance f_{nl} than the nominal design, but the robust design is less sensitive to imperfections as indicated by the smaller mean $m_{f_{\text{nl}}}$ and standard deviation $\sigma_{f_{\text{nl}}}$. A comparison of the linear and nonlinear statistics in Table 2 again shows that the effect of imperfections is significantly amplified by geometric nonlinear effects as the nonlinear mean and standard deviation are much larger than their linear counterpart.

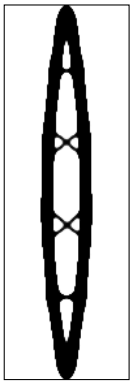

Figure 9: Pinned column: robust design.

Design	f_{nl}	$m_{f_{\mathrm{l}}}$	$\sigma_{f_{\mathrm{l}}}$	$\hat{m}_{f_{\mathrm{nl}}}$	$\hat{\sigma}_{f_{\mathrm{nl}}}$	$m_{f_{\mathrm{nl}}}$	$\sigma_{f_{\mathrm{nl}}}$	f_{Rnl}
Nominal	6.90	8.38	1.86	/	/	11.70	6.44	18.14
Robust	7.47	7.91	0.44	8.10	0.56	8.10	0.55	8.65

Table 2: Results for the optimized pinned column designs including the nominal nonlinear performance f_{nl}, the mean $m_{f_{\mathrm{l}}}$ and standard deviation $\sigma_{f_{\mathrm{l}}}$ of the linear compliance obtained by a Monte Carlo simulation with 10 000 samples, the estimated statistics at the end of the robust optimization $\hat{m}_f$ and $\hat{\sigma}_f$, the mean $m_{f_{\mathrm{nl}}}$ and standard deviation $\sigma_{f_{\mathrm{nl}}}$ of the nonlinear end-compliance, and the robust objective $f_{\mathrm{Rnl}} = m_{f_{\mathrm{nl}}} + \sigma_{f_{\mathrm{nl}}}$. All results are in kJ.

4. Conclusions

For structures with slender members in compression, geometric imperfections are an important concern and often have a significant impact on the structural performance. Slender structures are particularly sensitive, especially when stability and other geometric nonlinear effects are taken into account. This paper develops a robust approach to topology optimization in order to obtain well-performing designs that are also insensitive to imperfections. Geometric nonlinearities are taken into account by minimizing the end-compliance while using a Total Lagrangian formulation to model large displacements.

Geometric imperfections are modeled by means of a random field in the design domain. The objective function of the robust optimization problem is formulated as a weighted sum of the mean and standard deviation of the

structural performance affected by geometric imperfections. These stochastic moments are estimated using a second-order perturbation method during the optimization. The perturbation method relies on adjoint differentiation and a semi-analytical approach for computing the imperfection sensitivities. The computational cost of the method increases with the number of random variables and is therefore mainly suitable for strongly correlated random fields of imperfections. When the imperfections are weakly correlated and hence a large number of random variables is needed in the random field discretization, other uncertainty quantification techniques such as Monte Carlo simulation or adaptive methods [46] will be more efficient.

The robust approach is applied in two design problems. The structures in these applications, a shallow arch and a pinned column, exhibit different types of critical points. In both cases, however, it is seen that including imperfections in the nominal designs, which exhibit a linear response in their perfect state, trigger significant geometric nonlinear effects. As a result, the performance of the nominal designs is strongly affected by imperfections. Despite having a slightly worse nominal performance, the designs obtained by the robust approach are much less sensitive to geometric imperfections. In both problems, the second-order perturbation method provides relatively accurate estimates for the statistics of the robust designs. This is expected to hold for problems where the applied load is relatively small compared to the critical load of the structure. The approximation is likely to deteriorate as the load approaches the critical load where the response of the design is often indifferentiable with respect to imperfections.

5. Acknowledgments

The research presented in this paper has been performed within the framework of the KU Leuven - BOF PFV/10/002 OPTEC - Optimization in Engineering Center.

[1] J. Deaton, R. Grandhi, A survey of structural and multidisciplinary continuum topology optimization: post 2000, Structural and Multidisciplinary Optimization (2013) 1–38.

[2] O. Sigmund, K. Maute, Topology optimization approaches, Structural and Multidisciplinary Optimization 48 (6) (2013) 1031–1055.

[3] A. Ben-Tal, A. Nemirovski, Robust truss topology design via semidefinite programming, SIAM Journal on Optimization 7 (4) (1997) 991–1016.

[4] K. Brittain, M. Silva, D. Tortorelli, Minmax topology optimization, Structural and Multidisciplinary Optimization 45 (2012) 657–668.

[5] P. Dunning, H. Kim, Robust topology optimization: Minimization of expected and variance of compliance, AIAA Journal 51 (11) (2013) 2656–2664.

[6] A. Asadpoure, M. Tootkaboni, J. Guest, Robust topology optimization of structures with uncertainties in stiffness – Application to truss structures, Computers & Structures 89 (11-12) (2011) 1131–1141.

[7] S. Chen, W. Chen, S. Lee, Level set based robust shape and topology optimization under random field uncertainties, Structural and Multidisciplinary Optimization 41 (2010) 507–524.

[8] S. Chen, W. Chen, A new level-set based approach to shape and topology optimization under geometric uncertainty, Structural and Multidisciplinary Optimization 44 (2011) 1–18.

[9] X. Guo, W. Zhang, L. Zhang, Robust structural topology optimization considering boundary uncertainties, Computer Methods in Applied Mechanics and Engineering 253 (0) (2013) 356–368.

[10] F. Wang, B. Lazarov, O. Sigmund, On projection methods, convergence and robust formulations in topology optimization, Structural and Multidisciplinary Optimization 43 (2011) 767–784.

[11] M. Schevenels, B. Lazarov, O. Sigmund, Robust topology optimization accounting for spatially varying manufacturing errors, Computer Methods in Applied Mechanics and Engineering 200 (49-52) (2011) 3613–3627.

[12] M. Jansen, G. Lombaert, M. Diehl, B. Lazarov, O. Sigmund, M. Schevenels, Robust topology optimization accounting for misplacement of material, Structural and Multidisciplinary Optimization 47 (3) (2013) 317–333.

[13] M. Jalalpour, T. Igusa, J. Guest, Optimal design of trusses with geometric imperfections: Accounting for global instability, International Journal of Solids and Structures 48 (21) (2011) 3011–3019.

[14] B. Lazarov, M. Schevenels, O. Sigmund, Robust design of large-displacement compliant mechanisms, Mechanical Sciences 2 (2) (2011) 175–182.

[15] T. Buhl, C. Pedersen, O. Sigmund, Stiffness design of geometrically nonlinear structures using topology optimization, Structural and Multidisciplinary Optimization 19 (2000) 93–104.

[16] T. Bruns, O. Sigmund, D. Tortorelli, Numerical methods for the topology optimization of structures that exhibit snap-through, International Journal for Numerical Methods in Engineering 55 (10) (2002) 1215–1237.

[17] M. Ohsaki, K. Ikeda, Stability and Optimization of Structures: Generalized Sensitivity Analysis, Mechanical Engineering Series, Springer, 2010.

[18] M. Bendsøe, O. Sigmund, Topology optimization: Theory, Methods and Applications, 2nd Edition, Springer, Berlin, 2004.

[19] M. Bendsøe, Optimal shape design as a material distribution problem, Structural and Multidisciplinary Optimization 1 (1989) 193–202.

[20] G. Rozvany, M. Zhou, T. Birker, Generalized shape optimization without homogenization, Structural and Multidisciplinary Optimization 4 (1992) 250–252.

[21] J. Guest, J. Prevost, T. Belytschko, Achieving minimum length scale in topology optimization using nodal design variables and projection functions, International Journal for Numerical Methods in Engineering 61 (2) (2004) 238–254.

[22] O. Sigmund, Morphology-based black and white filters for topology optimization, Structural and Multidisciplinary Optimization 33 (4–5) (2007) 401–424.

[23] S. Xu, Y. Cai, G. Cheng, Volume preserving nonlinear density filter based on Heaviside functions, Structural and Multidisciplinary Optimization 41 (2010) 495–505.

[24] M. Jansen, B. Lazarov, M. Schevenels, O. Sigmund, On the similarities between micro/nano lithography and topology optimization projection methods, Structural and Multidisciplinary Optimization 48 (4) (2013) 717–730.

[25] B. Bourdin, Filters in topology optimization, International Journal for Numerical Methods in Engineering 50 (9) (2001) 2143–2158.

[26] T. Bruns, D. Tortorelli, Topology optimization of non-linear elastic structures and compliant mechanisms, Computer Methods in Applied Mechanics and Engineering 190 (26–27) (2001) 3443–3459.

[27] K. Svanberg, The method of moving asymptotes – A new method for structural optimization, International Journal for Numerical Methods in Engineering 24 (1987) 359–373.

[28] K. Choi, N. Kim, Structural sensitivity analysis and optimization, Volume 1. Linear systems, Springer, New York, 2005.

[29] M. Firl, K.-U. Bletzinger, Shape optimization of thin walled structures governed by geometrically nonlinear mechanics, Computer Methods in Applied Mechanics and Engineering 237–240 (0) (2012) 107–117.

[30] S. Krenk, Non-linear Modeling and Analysis of Solids and Structures, Cambridge University Press, 2009.

[31] P. Wriggers, Nonlinear Finite Element Methods, Springer-Verlag Berlin Heidelberg, 2008.

[32] O. Zienkiewicz, R. Taylor, The finite element method, Volume 2: solid mechanics, 5th Edition, Butterworth-Heinemann, Oxford, United Kingdom, 2000.

[33] A. Klarbring, N. Strömberg, Topology optimization of hyperelastic bodies including non-zero prescribed displacements, Structural and Multidisciplinary Optimization 47 (1) (2013) 37–48.

[34] T. Bruns, D. Tortorelli, An element removal and reintroduction strategy for the topology optimization of structures and compliant mechanisms, International Journal for Numerical Methods in Engineering 57 (10) (2003) 1413–1430.

[35] F. Wang, B. Lazarov, O. Sigmund, J. Jensen, Interpolation scheme for fictitious domain techniques and topology optimization of finite strain elastic problems, Computer Methods in Applied Mechanics and Engineering 276 (0) (2014) 453–472.

[36] G. Yoon, Y. Kim, Element connectivity parameterization for topology optimization of geometrically nonlinear structures, International Journal of Solids and Structures 42 (7) (2005) 1983–2009.

[37] M. Neves, H. Rodrigues, J. Guedes, Generalized topology design of structures with a buckling load criterion, Structural optimization 10 (2) (1995) 71–78.

[38] N. Pedersen, Maximization of eigenvalues using topology optimization, Structural and Multidisciplinary Optimization 20 (1) (2000) 2–11.

[39] M. Crisfield, Non-linear Finite Element Analysis of Solids and Structures, Volume 2: Advanced Topics, John Wiley & Sons, 1997.

[40] A. Nouy, A. Clément, F. Schoefs, N. Moës, An extended stochastic finite element method for solving stochastic partial differential equations on random domains, Computer Methods in Applied Mechanics and Engineering 197 (2008) 4663–4682.

[41] M. Baitsch, D. Hartmann, Optimization of slender structures considering geometrical imperfections, Inverse Problems in Science and Engineering 14 (6) (2006) 623–637.

[42] K. Kolanek, S. Jendo, Random field models of geometrically imperfect structures with "clamped" boundary conditions, Probabilistic Engineering Mechanics 23 (2-3) (2008) 219–226.

[43] C. Li, A. Der Kiureghian, Optimal discretization of random fields, Journal of Engineering Mechanics 119 (6) (1993) 1136–1154.

[44] H. Beyer, B. Sendhoff, Robust optimization – A comprehensive survey, Computer Methods in Applied Mechanics and Engineering 196 (33–34) (2007) 3190–3218.

[45] G. Schuëller, H. Jensen, Computational methods in optimization considering uncertainties – An overview, Computer Methods in Applied Mechanics and Engineering 198 (1) (2008) 2–13.

[46] O. Le Maître, O. Knio, Spectral Methods for Uncertainty Quantification: With Applications to Computational Fluid Dynamics, Scientific Computation, Springer, 2010.

[47] B. Lazarov, M. Schevenels, O. Sigmund, Topology optimization considering material and geometric uncertainties using stochastic collocation methods, Structural and Multidisciplinary Optimization 46 (4) (2012) 597–612.

[48] R. Ghanem, P. Spanos, Stochastic finite elements: a spectral approach, Springer-Verlag, New York, 1991.

[49] B. Sudret, A. Der Kiureghian, Stochastic finite element methods and reliability – A state-of-the-art report, Report UCB/SEMM-2000/08, Department of Civil & Environmental Engineering, University of California, Berkeley (November 2000).

[50] S. Arnout, M. Firl, K.-U. Bletzinger, Parameter free shape and thickness optimisation considering stress response, Structural and Multidisciplinary Optimization 45 (2012) 801–814.

[51] D. Tortorelli, P. Michaleris, Design sensitivity analysis: Overview and review, Inverse Problems in Engineering 1 (1) (1994) 71–105.